

## 主論文の要旨

A mutation in *DOK7* in congenital myasthenic syndrome forms aggresome in cultured cells, and reduces *DOK7* expression and MuSK phosphorylation in patient-derived iPS cells

先天性筋無力症候群における*DOK7*の変異は、培養細胞でアグリソーム形成を誘導し、患者由来iPS細胞で*DOK7*の発現とMuSKリン酸化を減少させる

名古屋大学大学院医学系研究科 総合医学専攻  
先端応用医学講座 神経遺伝情報学分野

(指導：大野 欽司 教授)

张 少川

## **【Introduction】**

Congenital myasthenic syndromes (CMS) are a heterogeneous group of rare inherited diseases characterized by muscle weakness and fatigue resulting from compromised signal transduction at the neuromuscular junction (NMJ). Mutations in a total of 34 genes have been reported to cause CMS. Within these gene molecules, the phosphorylation of MuSK plays a central role in the clustering of acetylcholine receptors (AChRs) at the motor endplate. Both defective and excessive phosphorylation of MuSK reduces AChR clusters.

*DOK7* enhances MuSK phosphorylation and mediate AChRs clustering. *DOK7* mutations account for 10-15% of CMS, and are the most common cause of limb-girdle myasthenia. *DOK7* is comprised of a pleckstrin homology (PH) domain, a phosphotyrosine-binding (PTB) domain, and a long unstructured C-terminal region containing a nuclear exporting signal (NES) and two tyrosine residues that can be phosphorylated. More than 70 missense, truncation, and splicing mutations have been reported in *DOK7* in CMS. Two reports showed that twelve missense mutations in *DOK7* (p.E3K, p.P31T, p.A33V, p.S45L, p.T77M, p.G109C, p.V139L, p.R158Q, p.G161R, p.G166R, p.G171D, and p.G180A) reduced the activity of *DOK7* on the MuSK phosphorylation. However, none reduced its expression and aggregate formations of mutant *DOK7* has not been investigated to date.

## **【Materials and Methods】**

We utilized patient-derived induced pluripotent stem cells (CMS-iPSCs) combined with a gene-editing tool, CRISPR/Cas9, to characterize two mutations, c.653-1G>C and c.190G>A (Figure 1). We also evaluate the effects of these mutations on protein expression, MuSK phosphorylation, and AChR clustering in *DOK7* transfected cells.

## **【Results】**

### **Activation of a cryptic 3' splice site in *DOK7* exon 6 due to c.653-1G>C at the 3' end of intron 5**

To examine the effects of c.653-1G>C on splicing, we analyzed *DOK7* transcripts in CMS-iPSCs (Figure 1). RT-PCR spanning *DOK7* exon 6 and sequencing of cloned fragments showed two aberrantly spliced transcripts in CMS-iPSCs (Figure 2A). One was due to skipping of exon 6, and the other was due to an activation of a cryptic splice site deleting seven nucleotides at the 5' end of exon 6 (Figure 2BC). The in-frame deletion lacking codons 218-257 (p.D218\_G257del) was similarly expressed compared to wild-type (WT)-*DOK7* in COS7 cells. The 7-nt-deleted transcript (c.653\_659delACCCAAG) predicting p.D218Afs\*34 showed markedly reduced expression in COS7 cells (Figure 2DE).

### **Effects of p.G64R on protein expression, AChR clustering, and MuSK interaction**

We next evaluated the effects of p.G64R on protein expression and AChR clustering in transfected C2C12 myoblasts. Western blotting showed that p.G64R significantly reduced its expression (Figure 3A). In differentiated C2C12 myotubes (Figure 3BC), WT-DOK7 induced AChR clustering but p.G64R-DOK7 had no activity on the clustering. As C2C12 myotubes express DOK7 endogenously, we used COS7 cells that express negligible amounts of DOK7 and MuSK. In co-immunoprecipitation assay with FLAG-tagged MuSK along with WT-DOK7 or p.G64R-DOK7 in COS7 cells (Figure 3D), G64R had no effect on the total amount of MuSK, but reduced the DOK7-associated MuSK. Similarly, tyrosine phosphorylation of MuSK was markedly reduced in p.G64R-DOK7-transfected COS7 cells.

### **Ubiquitin inhibitor MG132 accelerates the reduction of soluble p.G64R-DOK7 through forming insoluble aggregates**

The ubiquitin-proteasome system (UPS) is the major system for protein degradation. We next examined whether the UPS accelerated the clearance of p.G64R-DOK7 on mRNA or protein level. The proteasome inhibitor (MG132) had no effects on transcription but decreased the expression of p.G64R-DOK7 in transfected COS7 cells (Figure 4AB). This indicated that an accelerated UPS-mediated degradation of DOK7 was not the cause of the reduced expression of p.G64R-DOK7.

MG132 usually enhances protein degradation through autophagy activation, which is an alternative pathway to clear the irregularly folded or unfolded proteins. These improperly folded proteins tend to form insoluble aggregates. We thus examined whether p.G64R-DOK7 form a detergent-insoluble fraction. WT-DOK7 was mostly present in the detergent-soluble fraction, whereas p.G64R-DOK7 was mostly located in the detergent-insoluble fraction (Figure 4C). p.G64R also decreased the sum of the soluble and insoluble fractions of DOK7 (Figure 4D). MG132 treatment increased the amount of p.G64R-DOK7 in the insoluble fraction in dose- and time-dependent manners (Figure 4EF). Immunostaining of DOK7 in the COS7 cells also showed that p.G64R-DOK7 was prone to form aggregated puncta at the juxtannuclear region, whereas WT-DOK7 was diffusely dispersed in the cytoplasm (Figure 4GH). Nocodazole, an inhibitor of microtubule formation, markedly reduced the aggresome formations of p.G64R-DOK7 in COS7 cells (Figure 5A). p.G64R-DOK7 aggregates were recruited at the microtubule-organizing center (MTOC, Figure 5B) and colocalized with the aggresome markers (ubiquitin, parkin, P62, and HSP70, Figure 5CDE). These results suggested that p.G64R caused abnormal folding of DOK7, which made DOK7 ubiquitinated, transported to MTOC, and formed aggresomes at the juxtannuclear region.

### **Comparison of CMS-iPSCs with p.G64R and isogenic CMS-iPSCs<sup>Cas9</sup> without p.G64R**

To dissect the effect of p.G64R-DOK7 in patient-derived iPSCs, we established an isogenic cell line, CMS-iPSCs<sup>Cas9</sup>, from CMS-iPSCs by correcting c.190A>G (p.G64R), while retaining c.653-1G>C on another allele (Figure 6ABC). First, myogenic marker genes (*MYH3* and *MYOD1*) and NMJ-associated genes (*LRP4*, *DOK7*, *MUSK*, and *CHRNA3*) were induced in myogenic differentiation of both CMS-iPSCs and CMS-iPSCs<sup>Cas9</sup> (Figure 6D). Next, we observed that, in contrast to CMS-iPSCs<sup>Cas9</sup>, endogenous *DOK7* was undetectable even after immunoprecipitation (Figure 7A), and the phosphorylation of endogenous MuSK was markedly low in myogenically differentiated CMS-iPSCs (Figure 7B). In myogenically differentiated CMS-iPSCs, *DOK7* made aggregates at the juxtannuclear region (Figure 7CD). In contrast to COS7 cells, however, HSP70 was not colocalized with *DOK7*. Taken together, p.G64R reduced the expression of *DOK7* and MuSK phosphorylation, and formed aggregates at the juxtannuclear region in myogenically differentiated CMS-iPSCs.

### **【Discussion】**

We identified compound heterozygous mutations (c.653-1G>C and p.G64R) in *DOK7* in a patient with CMS. c.653-1G>C activated a cryptic 3' splice site in *DOK7* exon 6 and generated two abnormal transcripts. Both lacked the NES domain and the frame-shift transcript remove two key tyrosine residues. The deletion of the C-terminal region of *DOK7* in one or two alleles is observed in most *DOK7*-CMS patients, which markedly reduces the expression levels of *DOK7*. In addition, the disruption of the NES domain and the deletion of the C-terminal region in *DOK7* compromise *DOK7*-mediated MuSK phosphorylation and impair AChR clustering in C2C12 myotube. Since the lack of the C-terminal region of *DOK7* cause aberrantly small and simplified neuromuscular synapses in CMS, it largely compromises the NMJ formation but does not nullify the effect of *DOK7*.

We observed that p.G64R caused an overload to the UPS, and unprocessed p.G64R-DOK7 made aggresomes at the MTOC. Myogenically differentiated CMS-iPSCs showed that *DOK7* made aggregates at the juxtannuclear region without colocalization of HSP70. *DOK7* expression and MuSK phosphorylation were markedly reduced in the CMS-iPSCs. CRISPR/Cas9-mediated correction of p.G64R in CMS-iPSCs rescued these phenotypes. Lack of aggresomes in CMS-iPSCs was likely to be accounted for by high UPS activities in iPSCs. Alternatively, this was due to a technical constraint that iPSCs could not form mature myotubes compared to C2C12 myoblast. Although aggresomes were observed in cultured cells and possibly in CMS-iPSCs, the roles of aggresomes in the patient remain elusive.

### **【Conclusion】**

In this study, we reveal the pathogenic mechanisms of compound heterozygous mutations in CMS-patient. c.653-1G>C disrupted the normal splicing and generated two dysfunctional transcripts. c.190G>A generated residue substitution, p.G64R which interfered with protein folding. p.G64R-DOK7 makes aggresomes in cultured cells and is likely to compromise MuSK phosphorylation for AChR clustering in the CMS-patient.

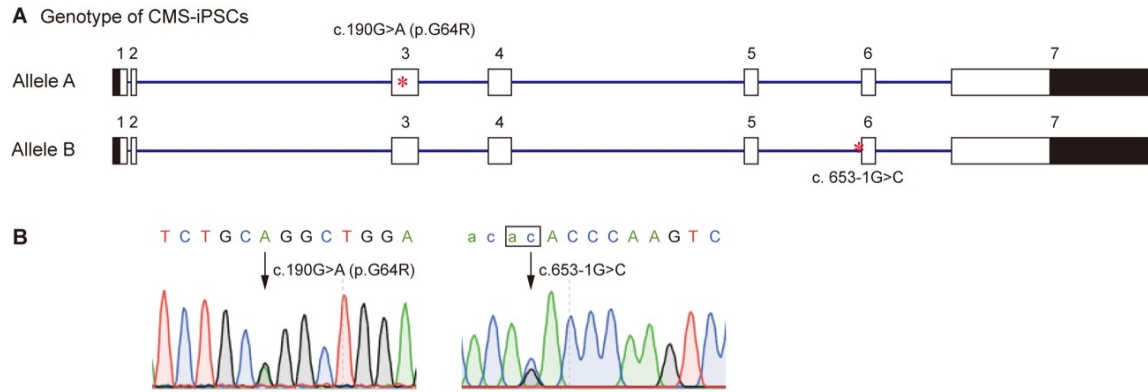


**Figure1. Mutations in *DOK7*.**

(A) Schematic of *DOK7* gene (NM\_173660.5) showing the location of mutations (red asterisks). The 5' and 3' untranslated regions are shown in black. (B) Sequencing chromatograms showing heteroallelic mutations. An invariant 'ag' dinucleotide at the 3' end of intron 5 is indicated by a box.

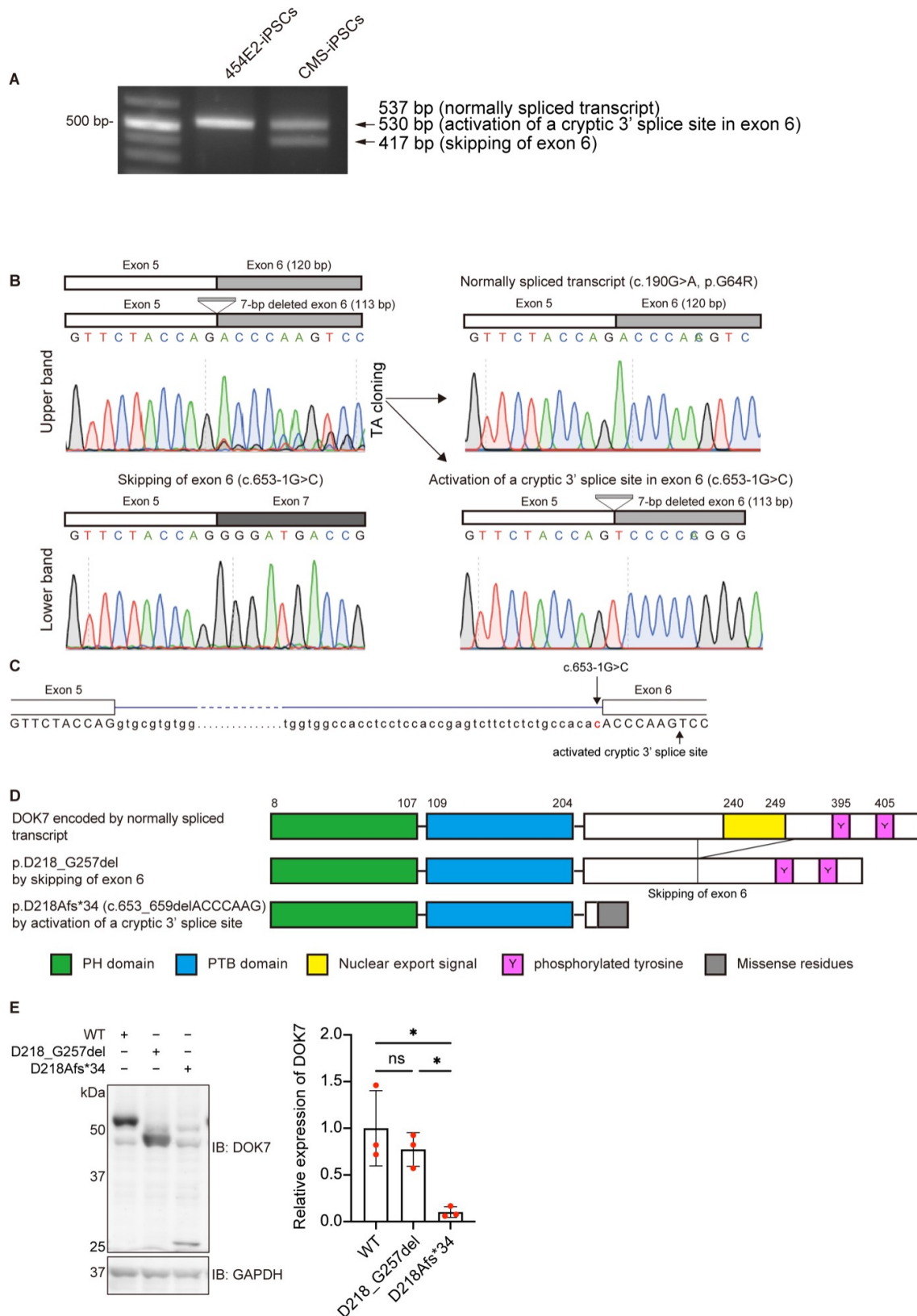


**Figure 2. Aberrantly spliced transcripts due to c.653-1G>C.**

(A) RT-PCR spanning *DOK7* exon 6 of control 454E2-iPSCs and patient-derived CMS-iPSCs. The upper band was comprised of 537-bp and 530-bp fragments. (B) Sequence chromatograms of three RT-PCR products in CMS-iPSCs. Chromatograms of the two transcripts in the upper band in A are indicated on the right. (C) Schematic showing the positions of the c.653-1G>C mutation and activated cryptic 3' splice site that is 7 nucleotides downstream of the intron 5/exon 6 junction. (D) Schematic presentation of *DOK7* proteins encoded by three transcripts in B. (E) Representative Western blotting and quantitative analysis of mutant *DOK7* arising from an allele with c.653-1G>C in transfected COS7 cells. Expression levels were normalized to that of GAPDH and to the ratio of wild-type (WT)-*DOK7*. Mean and SD ( $n = 3$  experiments) are indicated with individual values in red dots. One-way ANOVA with Dunnett's post hoc multiple comparison test was applied (ns, no significance;  $*p < 0.05$ ).

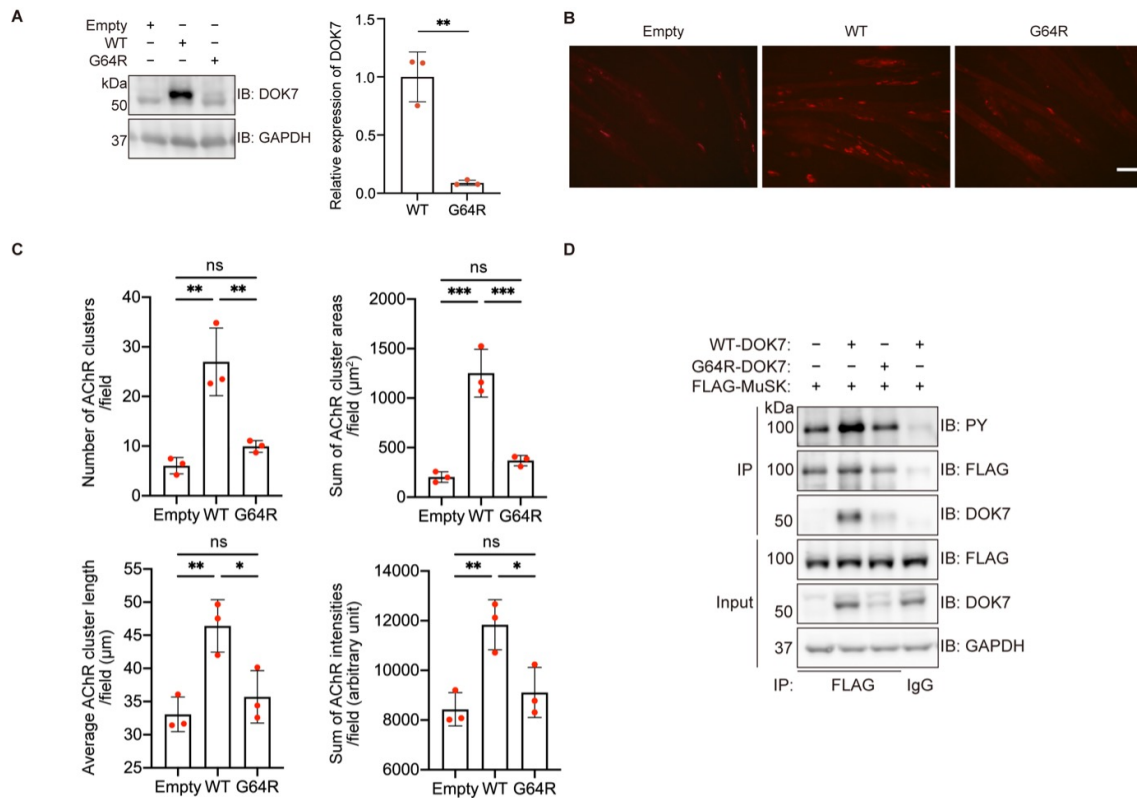


**Figure 3. Effects of p.G64R-DOK7 on protein expression, AChR clustering, and MuSK interaction.**

(A) Representative Western blotting and quantitative analysis of DOK7 in C2C12 cells transfected with wild-type (WT)-DOK7 or p.G64R-DOK7. Mean and SD ( $n = 3$  experiments) are indicated with individual values in red dots. Student's  $t$ -test ( $*P < 0.05$  and  $**P < 0.01$ ). (B) Transfection of wild-type (WT)-DOK7 but not p.G64R-DOK7 induced AChR clustering visualized by Alexa 594-conjugated  $\alpha$ -bungarotoxin (red) in C2C12 cells without agrin. Scale bar = 50  $\mu\text{m}$ . (C) Quantitative analysis of the number, total area, average length, and total signal intensity per visual field (0.143  $\text{mm}^2$ ) of AChR clusters in C2C12 cells expressing WT-DOK7 or p.G64R-DOK7. p.G64R-DOK7 markedly reduced AChR clustering. The mean values of 30 visual images are indicated by red dots. One-way ANOVA and Dunnett's multiple comparison test (ns, no significance;  $*p < 0.05$ ,  $**p < 0.01$ , and  $***p < 0.001$ ). (D) FLAG-MuSK were co-transfected with wild-type (WT)-DOK7 or p.G64R-DOK7 into COS7 cells. At 24 h after transfection, cell lysates were immunoprecipitated (IP) by anti-FLAG antibody, and followed by immunoblotting (IB) with the indicated antibody. PY, anti-phosphotyrosine antibody.

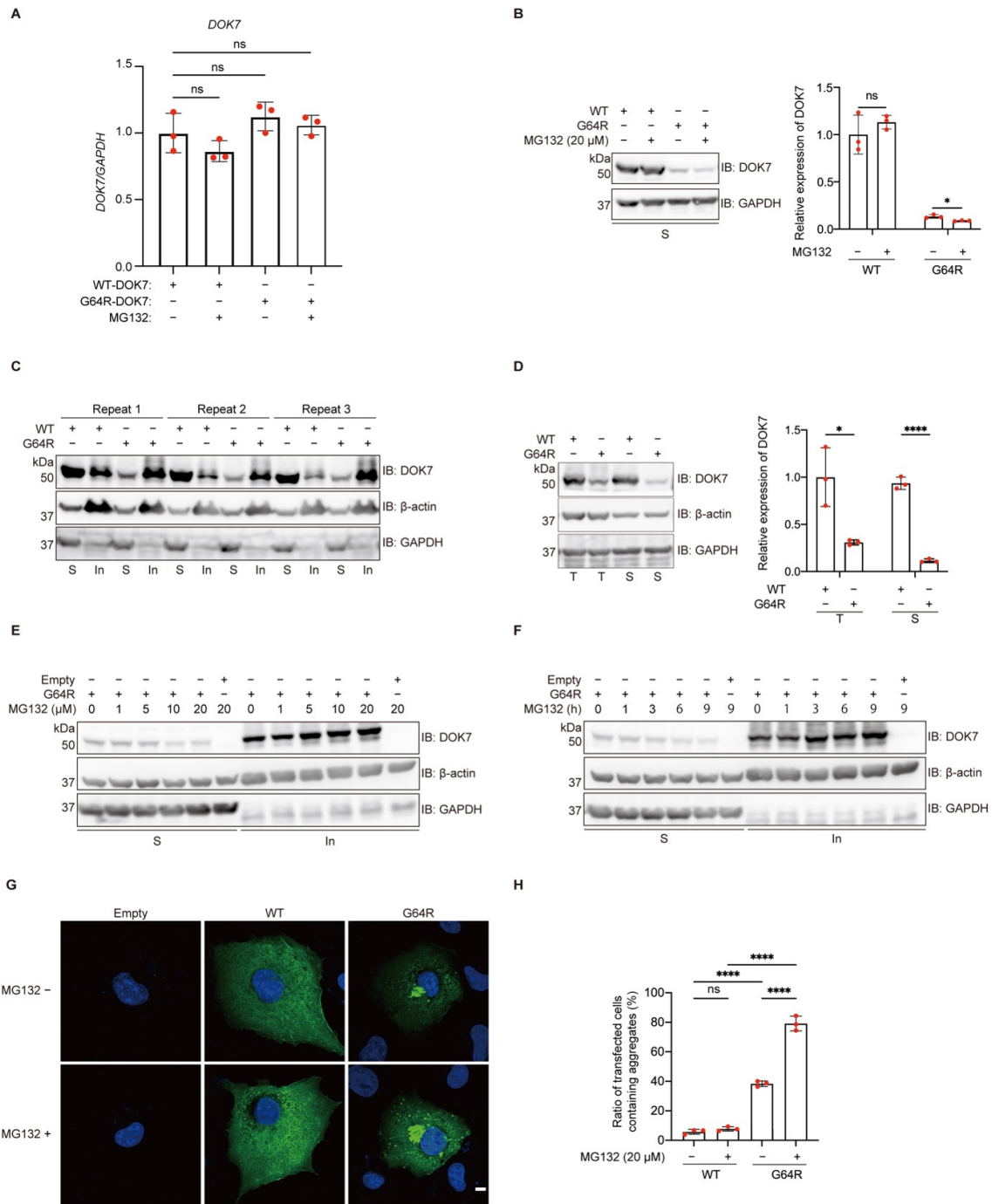


**Figure 4. Effects of p.G64R-DOK7 on mRNA expression, protein solubility, and aggregation after MG132 treatment.**

(A) At 18 h after transfection of COS7 cells with WT-DOK7 or p.G64R-DOK7, 10 μM MG132 was added for 3 h. Red dots indicate the ratio of *DOK7* mRNA normalized for *GAPDH* mRNA ( $n = 3$  independent experiments).  $P$ -value was 0.08 by one-way ANOVA, and Dunnett's multiple comparison test yielded no significance (ns) compared to WT-DOK7. (B and D) Representative Western blotting and quantitative analysis of DOK7 and GAPDH without β-actin (B) or with β-actin (D) in detergent-soluble fractions (S) and total protein lysates (T), in transfected COS7 cells. MG132 (20 μM) was added 3 h before harvesting cells (B). Expression levels were normalized to that of GAPDH, and also to the ratio of wild-type (WT)-DOK7. Mean and SD ( $n = 3$  experiments) are indicated with individual values in red dots. Multiple Student  $t$ -test was applied. (ns, no significance,  $*p < 0.05$ ,  $****p < 0.0001$ ). Triplicated (C) and representative (E and F) Western blotting of DOK7, β-actin, and GAPDH in detergent-soluble (S) and insoluble (In) fractions, in transfected COS7 cells. (E) MG132 at 0-20 μM was added 3 h before harvesting cells. (F) MG132 at 20 μM was added at indicated time points. (G) Representative images of WT-DOK7 and p.G64R-DOK7 treated with or without 20 μM MG132 treatment for 3 h in transfected COS7 cells. Green and blue signals represent DOK7 and DAPI, respectively. Scale bar = 10 μm. (H) The ratio of transfected COS7 cells with aggregates in each experiment is indicated in red dot. Each experiment is an average of five visual fields and is comprised of at least 100 cells. Mean and SD ( $n = 3$  experiments) are indicated. One-way ANOVA with Dunnett's multiple comparison test (ns, no significance;  $****p < 0.0001$ ).

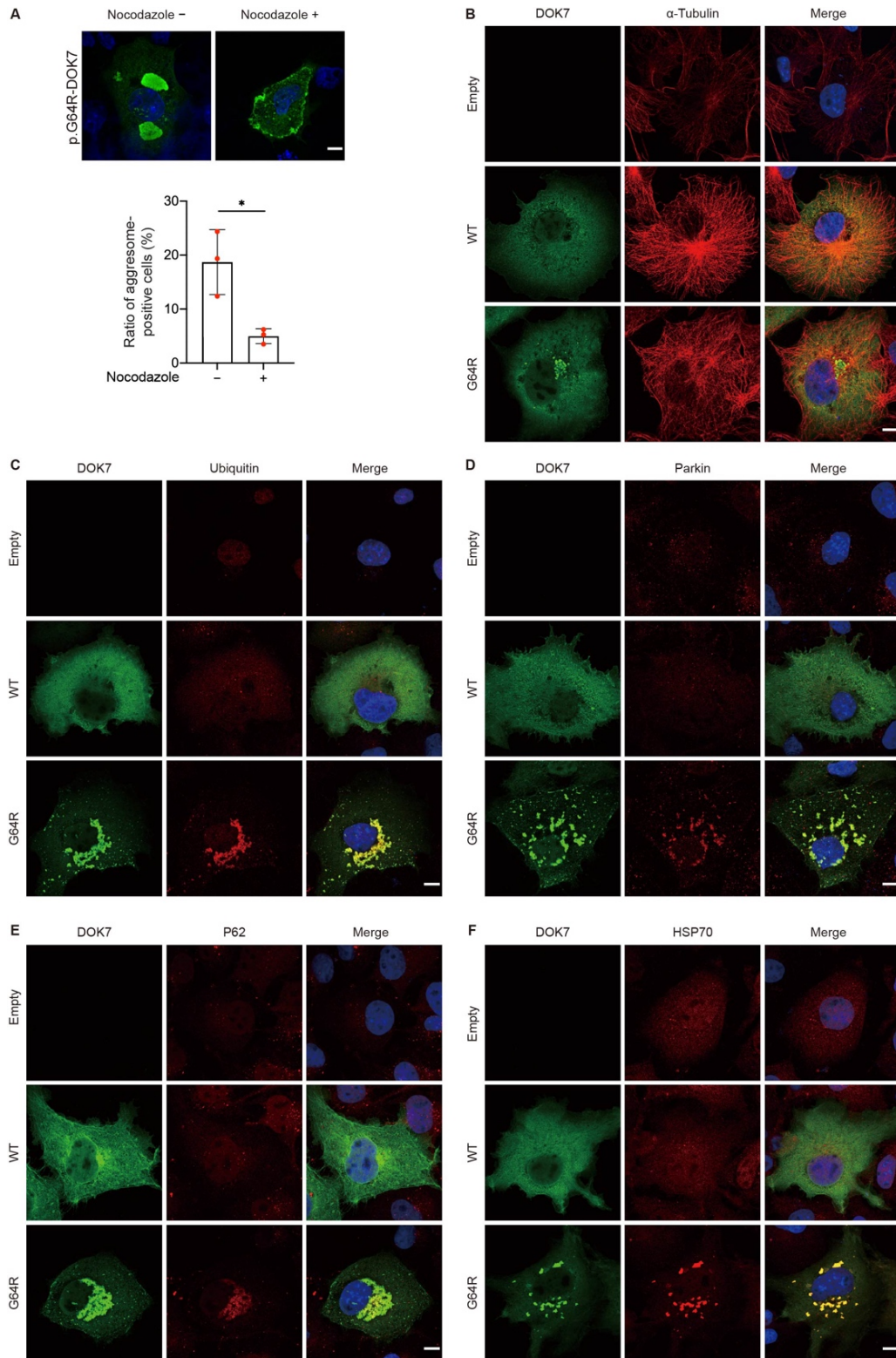


**Figure 5. Characterization of aggregates of p.G64R-DOK7.**

(A) Representative immunostaining of p.G64R-DOK7 in transfected COS7 cells with or without 10  $\mu$ M nocodazole, an inhibitor of microtubule polymerization. Scale bar = 10  $\mu$ m. The ratio of aggresome-positive cells after 10  $\mu$ M nocodazole treatment for 3 h in five visual fields is plotted in red for each experiment. Mean and SD ( $n = 3$  experiments) are indicated.  $*P < 0.05$  by Student's  $t$ -test. (B-E) Co-localization of DOK7 and aggresome markers of  $\alpha$ -tubulin (B), ubiquitin (C), parkin (D), P62 (E), and HSP70 (F). COS7 cells transfected with wild-type (WT)-DOK7 or p.G64R-DOK7 were immunostained with indicated antibodies at 18 h after transfection. Scale bar = 10  $\mu$ m.

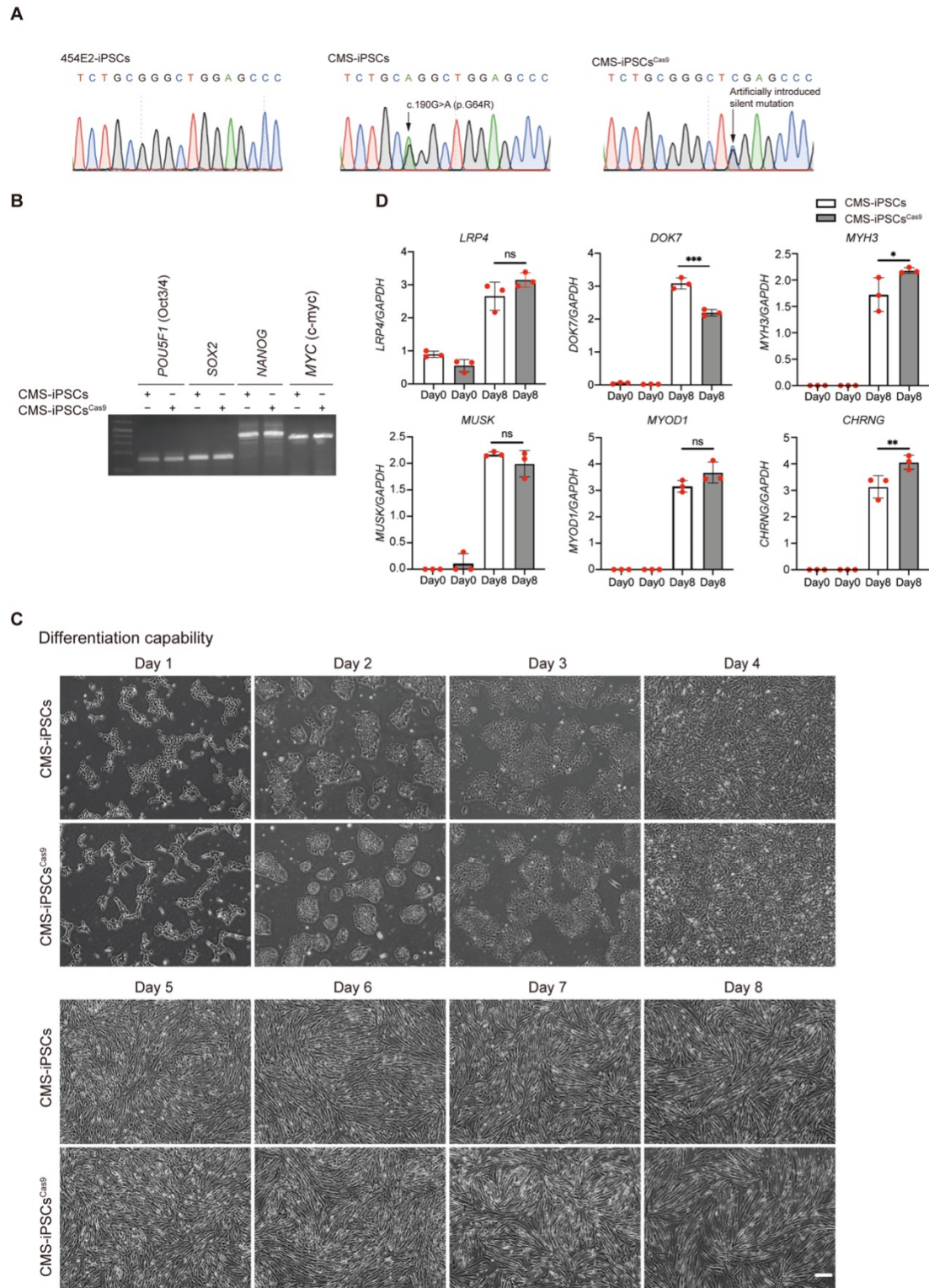


**Figure 6. Myogenic differentiation of iPSCs.**

(A) RT-PCR of pluripotency markers in control 454E2-iPSCs and patient-derived CMS-iPSCs. (B) Schematic illustration showing the workflow of iPSCs differentiation into myogenic cells. E8: Essential 8 Medium; DF: DMEM/F12 with 5% KSR;  $\alpha 5$ :  $\alpha$ MEM with 5% KSR; Puro: puromycin; Y: Y27632; SDN: SB431542, dorsomorphin, and N-acetyl-L-cysteine; C: CHIR99021; R: retinoic acid; Dox: doxycycline; and  $\beta$ -ME:  $\beta$ -mercaptoethanol. (C) Representative phase-contrast images of undifferentiated and myogenically differentiated iPSCs on day 8. Scale bar = 200  $\mu$ m.

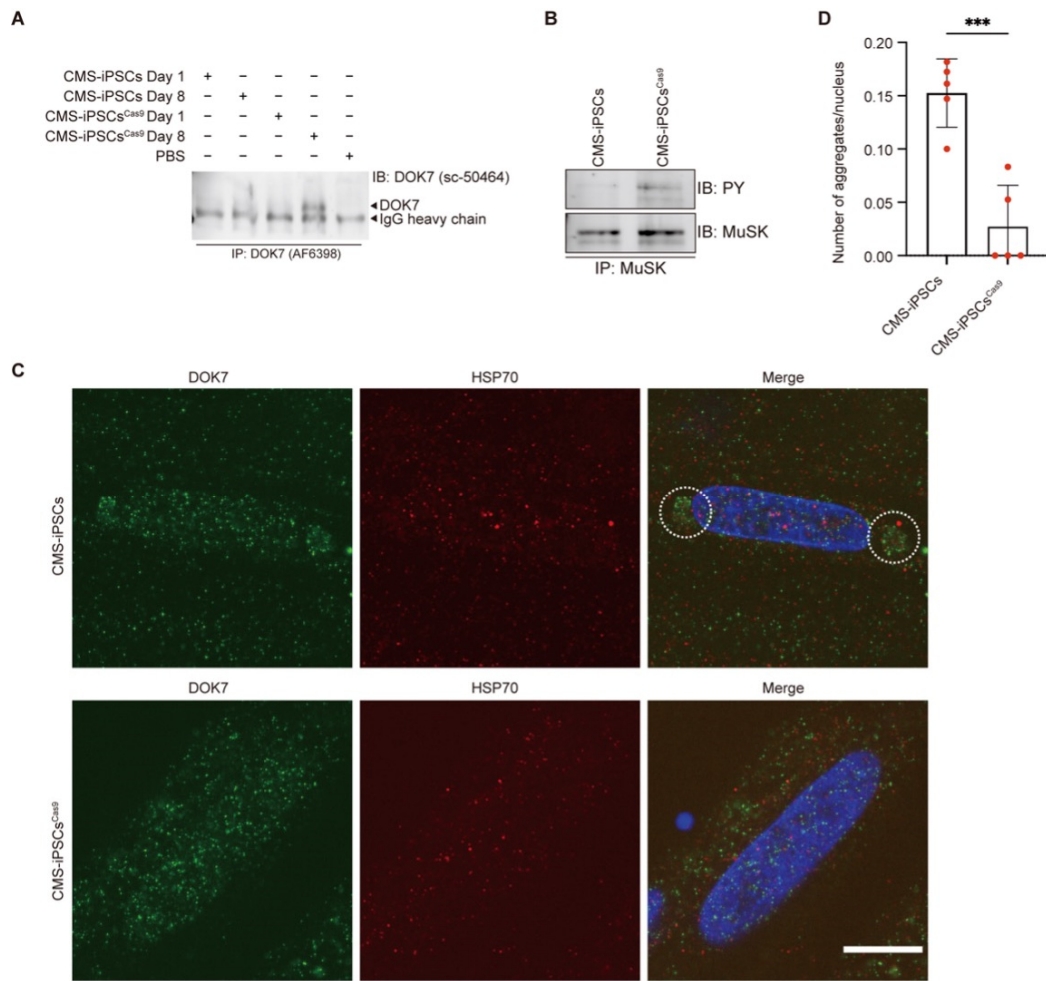


**Figure 7. The expression level of DOK7, the phosphorylation of MuSK, and the formation of aggregates in patient-derived CMS-iPSCs and isogenic CMS-iPSC<sup>Cas9</sup>.**

(A) Representative Western blotting of DOK7 in myogenically differentiated iPSCs on day 8. Low expression level of DOK7 necessitated the enrichment of DOK7 by immunoprecipitation (IP) before immunoblotting (IB). Anti-DOK7 antibodies are indicated in parentheses. (B) Phosphorylated MuSK was immunoblotted (IB) by an anti-phosphotyrosine antibody (PY) after immunoprecipitation (IP) of MuSK. (C) Representative immunostaining of DOK7 and HSP70 in CMS-iPSC- and CMS-iPSC<sup>Cas9</sup>-derived myogenic cells. Juxtannuclear aggregates are indicated by dotted circles. Scale bar = 10  $\mu$ m. (D) The number of juxtannuclear aggregates was blindly counted in five visual fields ( $\sim$ 30 nuclei each). Mean and SD are plotted. \*\*\* $P$  = 0.005 by Student's  $t$ -test.